Engineering Journal issn: 0125-8281

Article

Weiner Model Drop Test Identification of a Light Amphibious Airplane

Sinchai Chinvorarat

Department of Mechanical and Aerospace Engineering, Faculty of Engineering, King Mongkut's University of Technology North Bangkok, Bangkok, 10800, Thailand
E-mail: sinchai.c@eng.kmutnb.ac.th

Abstract. The new approach of the Weiner model for identifying drop test dynamics of a light amphibious airplane is presented in this paper. Unlike the traditional identification method of the Hammerstein model using LS-SVM with Gaussian radial basis serving as the kernel function, the small-signal excitation input is used to estimate the linear block of the Weiner model. Then, the static nonlinearity function of the model is identified through LS-SVM. The RMSE of the proposed Weiner model is 0.48805 and 0.38246 for the strut and wheel of the landing gear. The proposed Weiner model has better identification performance than the Hammerstein model and the traditional governing equation of the landing gear. The drop experiment of the light amphibious airplane is carried out not only to prove standard airworthiness compliance but also to verify the identifiability, accuracy, and performance of system identification.

Keywords: Weiner model, kernel function, small signal input, landing gear, light amphibious airplane.

ENGINEERING JOURNAL Volume 26 Issue 1
Received 27 October 2021
Accepted 27 December 2021
Published 31 January 2022
Online at https://engj.org/
DOI:10.4186/ej.2022.26.1.25

1. Introduction

The technique of system identification is concerned with the creation of mathematical models for dynamic systems from the data they receive and produce [1]. This technique has a wide range of applications, including economics, communication, system dynamics, and control and data collecting systems. Through the use of mathematical models, it is possible to get a better knowledge of a system's features, which may then be used to explain, predict, and regulate its behavior. To get the best possible system identification, it is essential to have a comprehensive understanding of the system's historical behavior, as well as to use properly chosen representation models and a systematic approach to system identification.

Nonlinearities exist to some extent in all real processes. When nonlinearities are weak, linear models can be used to forecast or design control systems. In today's literature [2–6], there are several methods for creating linear models. Linear models can only be used in a restricted range when nonlinearities are dominant. A nonlinear model identification should be employed if the process has a wide working range or behaves strangely. Using a rigorous first-principles formulation is an alternative to nonlinear system modeling [7–9]. Another technique for identifying processes is to use soft computing technologies.

The selection of an appropriate model structure is one of the most difficult problems in nonlinear system identification. A variety of designs are now available, including neural networks [10], block-oriented models [11], Volterra series [12], NARMAX models [13-14], and fuzzy models [15]. The simplicity and flexibility of block-oriented models make them attractive for modeling nonlinear dynamic systems [16–21]. Wiener and Hammerstein models have been shown to be capable of representing a paralyzed skeletal muscle [22], a limb reflex control system [23], a DC-DC converter [24], a heat exchanger system, and a superheater-desuperheater in a boiler system [26], as well as a thermal process [27]. Block-oriented models are used to implement current control techniques [28–32], as well as the capacity to estimate parameters.

The article investigates block-oriented models, a family of nonlinear representations composed of linear time-invariant (LTI) systems linked with nonlinear static functions (NL) [33]. The Wiener (LTI-NL), Hammerstein (NL-LTI), Wiener-Hammerstein (LTI-NL-LTI), and Hammerstein-Wiener (NL-LTI-NL) models are the most common in this category [34]. Numerous techniques for identifying these models are now available in the literature. Lopes dos Santos et al. [35] provide an intriguing categorization of contributions made during the past decade.

In 1979 and 1995, Vapnik [36,37] developed support vector machines (SVMs), which have since become an important component of machine learning research across the globe [38]. It is a fundamental collection of supervised learning techniques used for data categorization and regression that is often referred to as the SVM. With the proper kernel function, the SVM is capable of essentially mapping a nonlinear training function to a high-dimensional space and computing a hyperplane solution for the training function [39]. The hyperplane classifier may be able to segregate data in hyperplane without the need for real data transformation, which may save a significant amount of computing time and storage space over time. Consequently, the SVM can model any nonlinear function by mapping a nonlinear signal onto the hyperplane and solve for important parameters on the basis of a linear function using a nonlinear signal mapping technique [40-42].

Recently, Least Squares-Support Vector Machines (LS-SVM) have also been applied in the identification of Hammerstein and Weiner type systems. Ressendiz et al. [43] investigated the online detection of nonlinear systems using the LS-SVM method. Viana et al. [44] utilized nature-inspired optimization to find a nonlinear landing gear model in the frequency domain. Tarhouni et al. [45] developed a nonlinear identification method based on multi-kernel least support but restricted to just two kernel functions in the algorithm. Falck et al. [46] introduced Least-Squares Support Vector Machines for the identification of Weiner-Hammerstein systems. Sjoberg et al. [47] proposed two algorithms based on the best slit of a linear model applied to Wiener-Hammerstein models. Ding et al. [48] investigated the discharge coefficient of landing gear using a dynamic equation of motion and a comparison of CFD results on a model with a dynamic drop.

Several scholars have suggested a technique for identifying Hammerstein systems with limited memory using LS-SVM. Although many techniques are available in the literature for identifying Wiener type systems, one way suggested in some publications is to utilize a method for identifying Hammerstein type systems. It was found via simulations that this technique may provide inaccurate estimated results. Rather than that, this paper proposed a new approach for identifying Wiener type systems via the use of randomly small signal inputs. This method enables the estimation of the model's linear and nonlinear components independently, as well as the estimation of the system's overall parameters.

This article is structured as follows: Section 2 introduces the landing gear shock strut model of an amphibious aircraft. Due to the fact that the shock strut contained hydraulic fluid and nitrogen gas under pressure, the nitrogen gas functioned as a spring, and the hydraulic fluid flowed through the internal valve, creating resistive damping. The dynamics of shock struts in general are nonlinear and are seldom described by the governing equation of motion. Section 3 discusses block-oriented models of Hammerstein models as well as the mathematical foundations of the least squares supporting vector machine used to find the nonlinear model. Section 4 introduces a novel approach for acquiring the Weiner model's linear parameters and nonlinear function through a random small input method. Section 5 demonstrated the

amphibious airplane's drop test experiment, demonstrating the dynamic reaction of the real drop and identifying models with discussion. The last part summarizes the findings and discusses possible future research studies.

2. Model of a Shock Strut Landing Gear

Fig. 1. A light amphibious airplane with a shock strut suspension.

A retractable main landing gear with a shock strut as an absorption element has been designed and installed in a small amphibious aircraft in order to enhance safety and stability during routine or emergency landings on runways, as shown in Fig. 1. Figures 2 and 3 provide a schematic depiction of the shock strut. The primary construction of the shock strut is composed of aluminum alloy, which has the advantage of being lightweight and easy to manage. Nitrogen gas under pressure is contained in the lower chamber of the strut, while hydraulic fluid is contained in the upper chamber. Two flow control valves are in sequence at the tip of the piston. These valves control oil flow in both directions: the first valve's larger valve orifice controls retraction, while the second valve's smaller valve aperture regulates extension. The resulting hydraulic pressure decrease across the orifice opposes strut closure, and the resulting fluid turbulence absorbs and dissipates impact energy effectively [49].

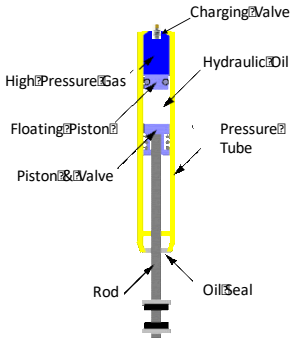

Fig. 2. Diagram of a shock strut.

The force generated inside the strut causes the fuselage body to accelerate, as well as the lower portion of the strut to accelerate and the tire to deflect [50]. It is self-evident that the strut and tire have a reciprocal effect on one another's behavior, and this must be taken into account while evaluating the system.

The total axial force owing to hydraulic resistance, nitrogen gas compression, and internal friction force is calculated as follows:

$$\begin{aligned} F_s &= (p_h - p_a)(A_1 - A_p) + p_a A_2 + F_f \\ &= (p_h - p_a)A_h + p_a A_a + F_f \\ &= F_h + F_a + F_f \end{aligned} \tag{1}$$

where A_1 denotes the inner cylinder's internal cross-sectional area, A_2 denotes the inner cylinder's external cross-sectional area, A_p denotes the rod's internal cross-sectional area, A_h denotes the hydraulic area, A_a denotes the pneumatic area, and $p_h - p_a$ denotes the pressure drop across the orifice. Thus, the total axial force is equal to the sum of the hydraulic force F_h, the pneumatic force F_a, and the friction force F_f.

The discharge coefficient (C_d) equation and the telescoping velocity may be used to calculate hydraulic force. When both compression and expansion strokes (s) are included, the hydraulic force may be represented as the following equation:

$$F_h = \frac{\dot{s}}{|\dot{s}|}\frac{\rho A_h^3}{2(C_d A_n)^2}\dot{s}^2 \tag{2}$$

The pneumatic force in the upper chamber is defined by the initial strut inflation pressure, the area subjected to the air pressure, and the instantaneous compression ratio in line with the polytrophic law of gas compression, which may be stated as follows:

$$F_a = p_{a_0} A_a \left(\frac{V_0}{V_0 - A_a s}\right)^n \tag{3}$$

where p_{a_0} denotes the gas pressure in the upper chamber of a completely expanded strut and V_0 denotes the gas volume of a fully extended strut. The axial friction force in the shock strut is equal to the total of the friction forces produced by each bearing connected to the inner and outer cylinders, and may be written as follows:

$$F_f = \frac{\dot{s}}{|\dot{s}|}(\mu_1|F_1| + \mu_2|F_2|) \tag{4}$$

When μ_1 is the friction coefficient for the upper bearing, F_1 is the normal force on the upper bearing, and μ_2 is the friction coefficient for the lower bearing, F_2 is the normal force on the lower bearing.

During the landing process, the vertical reaction force resulting from the tire compression can be expressed by:

$$F_v = (1 + C_T\dot{\delta})f(\delta) \tag{5}$$

where C_T is the tire vertical damping coefficient, δ is the tire hub vertical displacement, $\dot{\delta}$ is the tire hub vertical speed, and $f(\delta)$ is the tire static compression function.

Without consideration of the wheel rotation, the landing gear equation of motion can be expressed by:

$$m_1\ddot{z}_1 = m_1 g - (F_h + F_a + F_f)\cos\theta \tag{6}$$

$$m_2\ddot{z}_2 = m_2 g - \left(F_h + F_a + F_f\right)\cos\theta - F_v \quad (7)$$

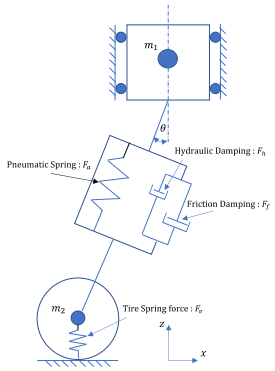

Fig. 3. Schematic diagram of landing gear.

The entire axial force produced inside the strut accelerates the fuselage body, as well as the lower portion of the strut, which accelerates and causes the tire to deflect. However, since the hydraulic force, pneumatic force, friction force, and tire reaction force are all inherently nonlinear functions, the landing gear's dynamic response can only be determined to a limited extent and with great difficulty. A candidate nonlinear identification model is proposed to identify and validate the dynamic response of the landing gear, in addition to solving the equation of motion of the landing gear in Eq. (6) and (7). The candidate nonlinear identification model provides a significantly more accurate model response than the traditional governing equation of motion.

3. Hammerstein Model Identification

Assuming the Hammerstein Model composes of the static nonlinearity cascade with the linear system as shown in Fig. 4 , the dynamics of the whole structure can be given as:

$$y_k = \sum_{i=1}^{n} a_i\, y_{k-i} + \sum_{j=0}^{m} b_j\, f\left(u_{k-j}\right) + e_k \quad (8)$$

where u_k and y_k denote the input and measured output. e_k denoted equation error and assumed to be white. m and n are the order of the numerator and denominator in the transfer function of the linear model. The model is so-called "nonlinear Auto-Regressive model with eXogeneous inputs" (NARX), which is one of the most studied model structures in the system identification [51].

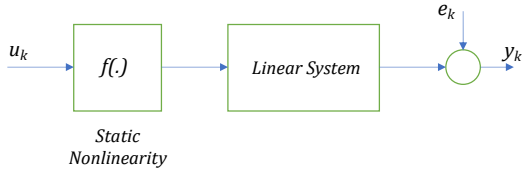

Fig. 4. Hammerstein Model.

In order to apply the least square support vector machines (LS-SVM) function estimation into the model [52], we assume the following structure for the static nonlinearity.

$$f(u) = w^T\varphi(u) + d \quad (9)$$

where $w \in \mathbb{R}$ and $d \in \mathbb{R}$ are unknown parameters to be found, and $\varphi(.)$ is called the feature map; its role is to map the data into a higher dimensional feature space, then Eq. (8) becomes:

$$y_k = \sum_{i=1}^{n} a_i\, y_{k-i} + \sum_{j=0}^{m} b_j\,(w)^T\varphi\left(u_{k-j}\right) + d + e_k \quad (10)$$

To estimate a_i, b_j, and f from a finite set of measurement, one can solve for the convex constraint optimization problem as follow:

$$\min_{w,a,b,d,e} \mathcal{F}(w,e_k) = \frac{1}{2}\|w\|^2 + \frac{\gamma}{2}\sum_{k=r}^{n} e_k^2 \quad (11)$$

$$s.t.$$

$$y_k = \sum_{i=1}^{n} a_i\, y_{k-i} + \sum_{j=0}^{m} b_j\,(w^T\varphi\left(u_{k-j}\right) + d) + e_k \quad (12)$$

where $r = max(m,n) + 1$, and γ is the regularization parameter. Ones can construct the Lagrangian to solve for the constraint optimization problem as follow:

$$\begin{aligned}\mathcal{L}(w,a,b,d,e_k,\alpha) &= \mathcal{F}(w,e_k) - \sum_{k=1}^{N}\alpha_k\left(\sum_{i=1}^{n} a_i\, y_{k-i}\right. \\ &\quad + \sum_{j=0}^{m} b_j\,(w^T\varphi\left(u_{k-j}\right) + d) \\ &\quad \left. + e_k - y_k\right)\end{aligned} \quad (13)$$

The optimization Eq. (13) is highly nonlinear, and it is almost impossible to find the solution without the known value of b_j . Therefore, the sub-optimization using collinearity constraint, by considering the coefficient b_j as a part of the SVM parameters, can make Eq. (10) as:

$$y_k = \sum_{i=1}^{n} a_i\, y_{k-i} + \sum_{j=0}^{m} w^T\varphi\left(u_{k-j}\right) + d + e_k \quad (14)$$

The new optimization problem become:

$$\min_{w_j,a,d,e_k} \mathcal{F}\left(w_j,e_k\right) = \frac{1}{2}\sum_{j=0}^{m} w_j^T w_j + \frac{\gamma}{2}\sum_{k=1}^{N} e_k^2 \quad (15)$$

$$s.t.$$

$$\sum_{i=1}^{n} a_i\, y_{k-i} + \sum_{j=0}^{m} w_j^T\varphi\left(u_{k-j}\right) + d + e_k - y_k = 0 \quad (16)$$

$$\sum_{k=1}^{N} w_j^T \varphi(u_k) = 0 \qquad (17)$$

with $k = r, \dots, N$ and $j = 0, \dots, m$

The constraint equation (17) is added up to the minimization problem to solve over parameterization, under the assumption that any set of constants can be added up to the nonlinear function as long as the sum of the constant is zero [53]. Now the corresponding Lagrangian can be written as:

$$\mathcal{L}(w_j, a, d, e_k, \alpha, \beta) = \mathcal{F}(w, e_k) - \sum_{k=1}^{N} \alpha_k \left(\sum_{i=1}^{n} a_i\, y_{k-i} + \sum_{j=0}^{m} w_j^T \varphi(u_{k-j}) + d + e_k - y_k \right) - \sum_{j=0}^{m} \beta_j \sum_{k=1}^{N} w_j^T \varphi(u_k) \qquad (18)$$

using the Karush-Kuhn-Tucher (KKT) conditions, we obtain the following equations.

$$\frac{\partial \mathcal{L}}{\partial w_j} = 0 \Longrightarrow w_j = \sum_{k=r}^{N} \alpha_k \varphi(u_k) + \beta_j \sum_{k=1}^{N} \varphi(u_k), \quad j = 0, \dots, m \qquad (19)$$

$$\frac{\partial \mathcal{L}}{\partial a_j} = 0 \Longrightarrow \sum_{k=r}^{N} \alpha_k\, y_{k-i} = 0, \quad i = 1, \dots, n \qquad (20)$$

$$\frac{\partial \mathcal{L}}{\partial d} = 0 \Longrightarrow \sum_{k=r}^{N} \alpha_k = 0 \qquad (21)$$

$$\frac{\partial \mathcal{L}}{\partial e_k} = 0 \Longrightarrow \alpha_k = \gamma e_k, \quad k = r, \dots, N \qquad (22)$$

$$\frac{\partial \mathcal{L}}{\partial \alpha_k} = 0 \Longrightarrow y_k = \sum_{i=1}^{n} a_i\, y_{k-i} + \sum_{j=0}^{m} w_j^T \varphi(u_{k-j}) + d + e_k, \quad k = 1, \dots, N \qquad (23)$$

$$\frac{\partial \mathcal{L}}{\partial \beta_j} = 0 \Longrightarrow \sum_{k=1}^{N} w_j^T \varphi(u_k) = 0, \quad j = 0, \dots, m \qquad (24)$$

From (19) and (24)

$$w_j^T \varphi(u_t) = \sum_{k=r}^{N} \alpha_k \varphi(u_k)^T \varphi(u_t) + \beta_j \sum_{k=1}^{N} \varphi(u_k)^T \varphi(u_t), \quad t = 1, \dots, N \qquad (25)$$

Lemma: (Primal-dual derivation), given system (12), the LS-SVM estimates for the nonlinear functions $w_j^T \varphi(u_t)$: $\mathbb{R} \to \mathbb{R}$, $j = 0, \dots, m$ are given as:

$$w_j^T \varphi(u_t) = \sum_{k=r}^{N} \alpha_k K(u_{k-j}, u_t) + \beta_j \sum_{k=1}^{N} K(u_k, u_t) \qquad (26)$$

where the parameters $\alpha_k, k = r, \dots, N, \beta_j, j = 0, \dots, m$, $a_i, i = 1, \dots, n$, and d can be obtained from the following set of linear equations:

$$\begin{bmatrix} 0 & 0 & 1_N^T & 0 \\ 0 & 0 & y_p & 0 \\ 1 & y_p^T & K + \gamma^{-1} I_N & K^0 \\ 0 & 0 & {K^0}^T & 1_N^T \Omega 1_N I_{m+1} \end{bmatrix} \begin{bmatrix} d \\ a \\ \alpha \\ \beta \end{bmatrix} = \begin{bmatrix} 0 \\ 0 \\ y_f \\ 0 \end{bmatrix} \qquad (27)$$

where $y_f = [y_r \quad \cdots \quad y_N]^T$,

$1_N = [1 \quad \cdots \quad 1]^T$,

$$y_p = \begin{bmatrix} y_{r-1} & y_r & \cdots & y_{N-1} \\ y_{r-2} & y_{r-1} & \cdots & y_{N-2} \\ \vdots & \vdots & \ddots & \vdots \\ y_{r-n} & y_{r-n+1} & \cdots & y_{N-n} \end{bmatrix}$$

$\alpha = [\alpha_r \quad \cdots \quad \alpha_N]^T$, $\beta = [\beta_0 \quad \cdots \quad \beta_m]^T$

$$K^0(p, q) = \sum_{k=1}^{N} \Omega_{k, r+p-q},$$

$$K(p, q) = \sum_{j=0}^{m} \Omega_{p+r-j-1, q+r-j-1}$$

There are many distinct kinds of kernel functions, including polynomial, Gaussian Radial Basis Function, exponential radial function, multi-layer perceptron, and others. When these kernels are used to classify the hyperplane, each kernel represents the data relationships in a distinct manner. Because of the dynamic model's inherent inner-connection of nonlinear dynamic signal and measurement noise, it is expected to be Gaussian noise with zero mean and limited variance, as stated in (10); as a result, using the Gaussian Radial Basis function to separate and regress data will provide higher data classification than using other types of the kernel. The Gaussian Radial Basis kernel used in this study has the following representation:

$$\Omega = K(x_t, x_k) = exp\left(-\frac{\|x_t - x_k\|^2}{2\sigma^2} \right) \qquad (28)$$

where σ is a deviation constant.

4. Weiner model Identification

Assuming the Weiner Model composes of the linear system cascade with the static nonlinearity as shown in Fig. 5, the dynamics of the whole structure can be given as:

$$z_k = \sum_{i=1}^{n} a_i\, z_{k-i} + \sum_{j=0}^{m} b_j\, u_{k-j} \qquad (29)$$

$$y_k = f(z_k) + e_k \qquad (30)$$

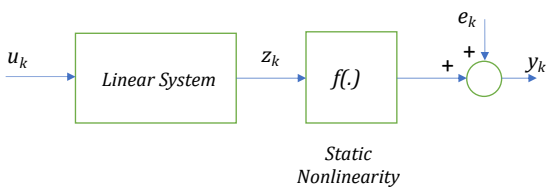

Fig. 5. Weiner Model.

$$u_k = \sum_{i=1}^{m} b_i\, u_{k-i} + \sum_{j=1}^{n} w_j^T\, \varphi(y_{k-j}) + d + e_k \qquad (31)$$

$$\min_{w,b,d,e_k} \mathcal{F}(w, e_k) = \frac{1}{2}\|w\|^2 + \frac{\gamma}{2}\sum_{k=r}^{n} e_k^2 \qquad (32)$$

$$s.t.$$

$$u_k = \sum_{i=1}^{m} b_i\, u_{k-i} + \sum_{j=1}^{n} w_j^T\, \varphi(y_{k-j}) + d + e_k \qquad (33)$$

$$\begin{bmatrix} 0 & 0 & 1_N^T & 0 \\ 0 & 0 & u_p & 0 \\ 1 & u_p^T & K + \gamma^{-1} I_N & K^0 \\ 0 & 0 & {K^0}^T & 1_N^T \Omega 1_N I_{m+1} \end{bmatrix} \begin{bmatrix} d \\ b \\ \alpha \\ \beta \end{bmatrix} = \begin{bmatrix} 0 \\ 0 \\ u_f \\ 0 \end{bmatrix} \qquad (34)$$

where $u_f = [u_r \quad \cdots \quad u_N]^T$,

$1_N = [1 \quad \cdots \quad 1]^T$,

$\alpha = [\alpha_r \quad \cdots \quad \alpha_N]^T$,

$$u_p = \begin{bmatrix} u_{r-1} & u_r & \cdots & u_{N-1} \\ u_{r-2} & u_{r-1} & \cdots & u_{N-2} \\ \vdots & \vdots & \ddots & \vdots \\ u_{r-m} & u_{r-m+1} & \cdots & u_{N-m} \end{bmatrix}$$

$\alpha = [\alpha_r \quad \cdots \quad \alpha_N]^T$, $\beta = [\beta_0 \quad \cdots \quad \beta_n]^T$,

$b = [b_0 \quad \cdots \quad b_m]^T$

$$K^0(p,q) = \sum_{k=1}^{N} \Omega_{k,r+p-q},$$

$$K(p,q) = \sum_{j=0}^{n} \Omega_{p+r-i-1,q+r-i-1}]$$

$$\Omega_{i,j} = K(y_i, y_i) = \varphi(y_i)^T \varphi(y_j) = exp\left(-\frac{\|y_i - y_j\|^2}{2\sigma^2}\right) \qquad (35)$$

While constructing the kernel matrix in Eq. (35), the noise in the input is mapped to an infinite dimension, which is a highly nonlinear mapping. Small magnitude noise may lead to extremely different mappings from the case that there is noise. To identify the Weiner model, a novel approach based on random tiny signal excitation, or equivalently, linearization of nonlinear functions around some operational point, has been presented. Assume that a nonlinear function is a piecewise function defined by its break points and the slope of the function between them. If the linear part's output stays constant between these places, we may represent the nonlinearity using a linear function. The nonlinear function may therefore be treated as a constant gain function, and the whole structure becomes a linear system. By selecting a suitably tiny input signal, we may compel the linear part's output to be between the piecewise function's break points. As a consequence, the system will be treated as a linear model multiplied by a constant gain, and the linear component of the Weiner model may be estimated as indicated in Fig. 6.

However, the issue of how tiny a magnitude signal is required to ensure that nonlinear is comparable to constant gain emerges. A strategy described in this study is to choose a tiny random signal and apply it to the system initially. This little random signal is amplified by constant K and applied to the system once again, while monitoring both output signals. If the amplitude of the second output signal of the recognized model is close to the K time of the first, we can most likely identify the linear portion; if not, we can further identify the model using just the input signal that remains in the margin of the final input signal. Once the linear component of the Weiner model is estimated using SVM, the nonlinear part may be recognized by feeding the output of the estimated linear part and the output of the original model into the SVM block to identify the nonlinear section, as illustrated in Fig. 7.

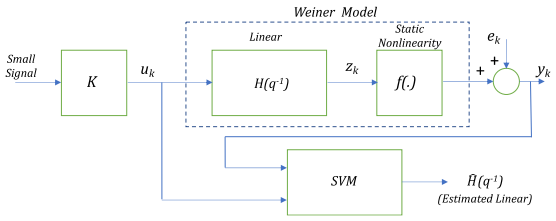

Fig. 6. Estimated linear part of Weiner model by small input method.

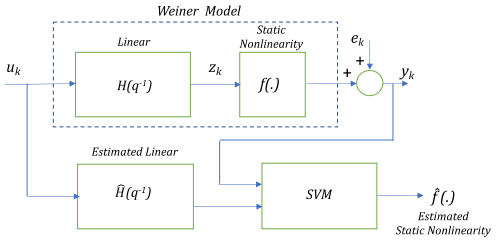

Fig. 7. Estimated static nonlinearity part of Weiner model.

Step for computing the proposed Weiner model

1. Apply a small amplitude signal randomly to the system and record the output.
2. Multiply the signal from (1) by a constant and apply it to the system.
3. The magnitude of the system's output signal was observed to see if it was close to the output from (1). If it is, keep applying the signal from (2) and recording the output.
4. If it is not, stop the input and record the last output, then choose the magnitude of the input signal so that it remains within the margin of the last input signal step in (3).
5. Use SVM identification method equations (15) to (27) to estimate the parameters of the linear part.

6. Increase the amplitude of the input signal and apply it to the system, then record the output signal.
7. Apply the same signal from (6) to the estimated linear part in (5).
8. The signal from (7) and (6) becomes the input/output to identify the static nonlinearity using the SVM regression algorithm.
9. Terminate the training of the SVM when the acceptable RMSE is achieved.
10. The parameters in (5) and the SVM in (9) represent the Weiner system.

5. Drop Test Experiment and Identification

A drop test is conducted in the test rig without the wheel moving. Figure 8 shows the test apparatus used to test the landing gear construction. The structure is put to the test. An aircraft body is held in place by two rings' fixtures, and a frictionless sliding mechanism is attached to the rings' fixtures to perform the drop test. During the drop test, three tiny wheel platforms with load cells record the initial weight and impact force. Two light sensors measure the wheel and strut displacement from the ground for each main landing gear. The data logger gathers and analyzes the data gathered from the light sensor and load cell to determine the aircraft's motion [54].

Fig. 8. Drop test rig.

The drop height required to validate the landing gear's strength is $h = 3.6\sqrt{\left(\frac{W}{S}\right)}$, where $\frac{W}{S}$ is wing loading, according to ASTM F-2245's drop test section 5.8.1. The load factor is calculated using the equation $n_j = \frac{h+\frac{d}{3}}{0.5*d_{tire}+0.65*d_{shock}}$, where d_{tire} is tire travel, d_{shock} is shock absorber travel, and d is the sum of $d_{tire} + d_{shock}$. The wing loading is equal to 10.54 lbs./sq.ft. for an airplane with a maximum takeoff weight of 1430 lbs. or 650 kg and a wing area of 140.85 sq. ft., resulting in a maximum drop height of 11.69 feet (approximately 300 mm.) and the landing gear must demonstrate compliance with the limited drop height without causing any damage.

The full-body light amphibious aircraft drop test begins with the configuration shown in Table 1. The air pressure for both tires on the main wheel is 25 psig, while the air pressure for the nose wheel is 20 psig. The 650 kg light amphibious aircraft features a 10% nose gear and a 90% main gear weight distribution. Both struts have a 100 mm initial stroke when the amphibious plane's landing gear is on the platform. At each drop point – 200, 250, and 300 mm – the amphibious aircraft is lifted by the hoist and free-falls to the platform. The results of each major landing gear drop test are shown in Tables 2 and 3. The peak load at the 200 mm drop height is 831.92 kgf on the left and 813.38 kgf on the right, resulting in a 2.53 G real impact load factor. With an actual impact load factor of 3.85 G, the peak load for left gear is 1,222.05 kgf and for right gear is 1,282.90 kgf at 250 mm drop height. Finally, with an actual impact load factor of 4.8 G, the peak load on left gear is 1568.42 kgf and 1,555.09 kgf at 300 mm drop height.

Table 1. Drop initial test parameters.

Effective Drop Weight *(We)*	Design Max. Strut Stroke *(Smax)*	Design Min Strut Stroke *(Smin)*	Init. Strut Stroke *(Sint)*	Init. Gas Pressure *(Pint)*	Diameter of Strut Retracted Oil-hole *(Dr)*	Diameter of Strut Extened Oil-hole *(De)*	Wheel Diameter (D,wheel)
650 kg	200 mm	20 mm	100 mm	0.8 Mpa	12 mm	8.5 mm	240 mm

Table 2. Drop test result measured at the left main landing gear.

Left Main Landing Gear						
Test Number	Drop Height (H)	Strut Stroke Travel *(d,strut)*	Tire Deflation Travel *(d ,tire)*	Peak Vertical Load *(Fp)*	Strut Energy Absorption *(Es)*	Tire Energy Absorption *(Et)*
1	200 mm	56.12 mm	31.73 mm	831.92 kgf	596.72 J	172.67 J
2	250 mm	94.43 mm	47.01 mm	1222.05 kgf	1060.74 J	250.06 J
3	300 mm	97.85 mm	52.47 mm	1568.42 kgf	1305.97 J	356.36 J

DOI:10.4186/ej.2022.26.1.25

Table 3. Drop test result measured at the right main landing gear.

Right Main Landing Gear						
Test Number	Drop Height (H)	Strut Stroke Travel *(d,strut)*	Tire Deflation Travel *(d,tire)*	Peak Vertical Load *(Fp)*	Strut Energy Absorption *(Es)*	Tire Energy Absorption *(Et)*
1	200 mm	55.53 mm	28.76 mm	813.38 kgf	587.92	146.55
2	250 mm	89.51 mm	39.19 mm	1282.9 kgf	1036.93	202.56
3	300 mm	87.78 mm	41.36 mm	1555.09 kgf	1174.71	251.29

Based on the data collection system's sampling rate of 1,000 Hz, the impact load of landing gear on a time scale at a drop height of 300 mm, as shown in Fig. 9, is the height required to pass the drop test standard. The total number of data points collected in the data logger is 2,000, and the drop test scenario was completed in 2 seconds. Because no absorption element is placed in the nose gear, there is no damp on the nose wheel. However, the peak load on the nose gear is very modest when compared to the peak force on the two main gears, indicating that the current nose gear design can certainly sustain the impact load during landing.

The relative displacement of the wheel and strut on both landing gears is shown in Fig. 10 on a time scale starting with the commencement of the drop test. It indicates the entire stroke range of the strut and wheel, as well as the associated settling time, when the impact load is applied. Notably, the settling time for both the left and right struts is less than 2 seconds. This impact absorption settling time performance guarantees the design landing gear's safety and stability. Figure 11 illustrates the dropped airplane's step motion in order to demonstrate the rebound of the tire and shock strut before and after impact with the platform. At the 300 mm. drop height, the tire is almost flat by the time the impact force reaches its maximum, yet the rim is not damaged when the tire bounces back to normal.

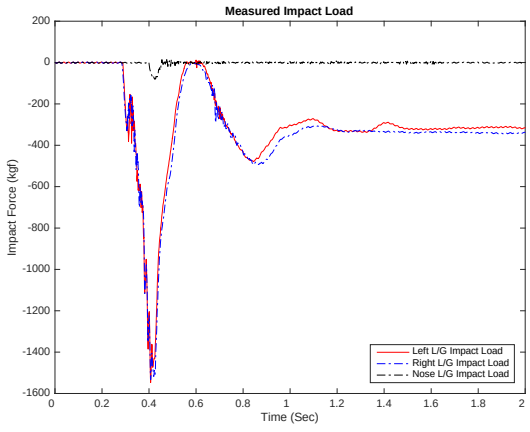

Fig. 9. Impact load of the nose gear and the main gear at 300 mm. drop height.

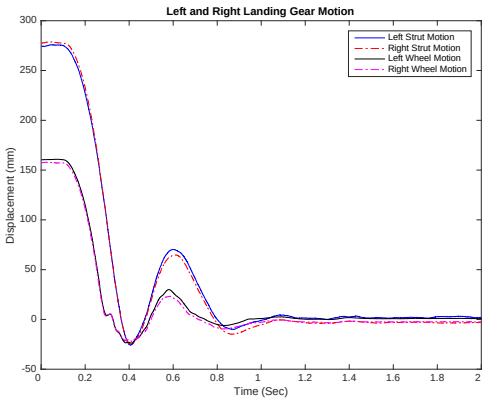

Fig. 10. The relative displacement of strut and wheel of the main landing gear was measured at 300 mm. drop height.

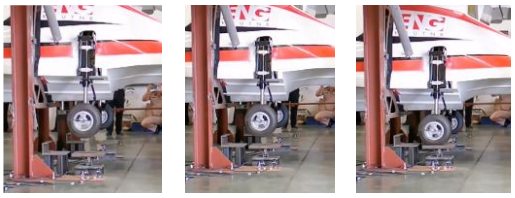

a) initial release b) falling c) first impact

d) recoiled e) extended

Fig. 11. Drop test motion in step.

The initial 200 data points of impact force input and displacement of the strut and wheel outputs of the landing gear are utilized to train the Hammerstein model. It should be noted that the training data starts when the wheel begins to touch the platform, which corresponds to the relative drop time of 0.28 seconds in Fig. 9. The Hammerstein identification method addresses the convex constraint optimization problem by using Gaussian radial basis multi-kernel functions under the KKT condition.

For the proposed Weiner identification method, start by exciting the model (strut and wheel) with a small force and observing the output. Then multiply the small force by K, excite the model, and observe the output. We can use these input and output signals to estimate the parameters of the linear part as mentioned in the algorithm steps. Once we can identify the linear part, then we can use the initial 200 data points of impact force input and

displacement of strut and wheel outputs to identify the nonlinear part as described in Fig. 7. Table 4 shows the estimated parameters of the Weiner model's linear part on both struts and wheels, and Fig. 12 and 13 show the static nonlinearity of the strut and wheel, respectively.

From the estimated linear parameters given in Table 4, one can observe that the linear identification on both strut and wheel is of order 6, which comes from trial numbers that gave the proper estimation of the output dynamic. However, one can achieve better estimation by increasing the model order, but it will consume more computational time and probably experience a slow convergence of the solution.

The motion of the actual drop test of the right strut, the Hammerstein model identification, the proposed Weiner model identification, and motion from the equation of motion with regard to a time scale spanning from zero to one second are illustrated in Fig. 14. The RMSE from the equation of motion compared with the actual motion is 9.7364, which is quite high due to the poor approximated parameters used in Eq. (2), (3), and (4). The Hammerstein model and the Weiner model, however, have given better identification with an RMSE of 0.88522 and 0.48805, respectively. Figure 15 also shows the measured displacement of the right wheel along with the Hammerstein model identification, the proposed Weiner model identification, and motion from the equation of motion with regard to a time scale spanning from zero to one second. The RMSE from the equation of motion compared with the actual motion is 11.3473. The RMSE of the Hammerstein model is 0.71204 and the RMSE of the Weiner model is 0.38246. Figure 16 illustrates the error of the Hammerstein model and the Weiner model relative to the actual strut motion, and Fig. 17 also shows the error of the Hammerstein model and the Weiner model relative to the actual wheel motion. There are lots of improvements in error reduction from the Hammerstein model to the Weiner model, which emphasizes that the new approach for estimating the Weiner model by small input technique works well in this landing gear drop test study.

The intricacy of the strut's internal structural components, as well as the nonlinearity of the shock strut's axial force, leads us to infer that the strut's identifiability is less accurate than that of the wheel in this situation. However, the accuracy of the identified Weiner model is better than that of the identified Hammerstein model, and the errors of both identified models are within acceptable limits, making them useful for predicting the drop dynamics of the airplane in other landing circumstances than we described here.

Table 4. Estimated linear parameters of Weiner model on both strut and wheel.

Linear Parameters of Weiner Model			
Strut		*Wheel*	
$a_0 = 0.4827$	$b_0 = -0.0053$	$a_0 = 0.2458$	$b_0 = -0.2185$
$a_1 = 1.0492$	$b_1 = -0.2028$	$a_1 = 0.8868$	$b_1 = -0.7919$
$a_2 = 0.0452$	$b_2 = 0.819$	$a_2 = 0.2674$	$b_2 = 0.2883$
$a_3 = -0.2931$	$b_3 = -0.5367$	$a_3 = 0.4235$	$b_3 = 0.492$
$a_4 = -0.2319$		$a_4 = -0.4633$	
$a_5 = -0.0522$		$a_5 = -0.3624$	

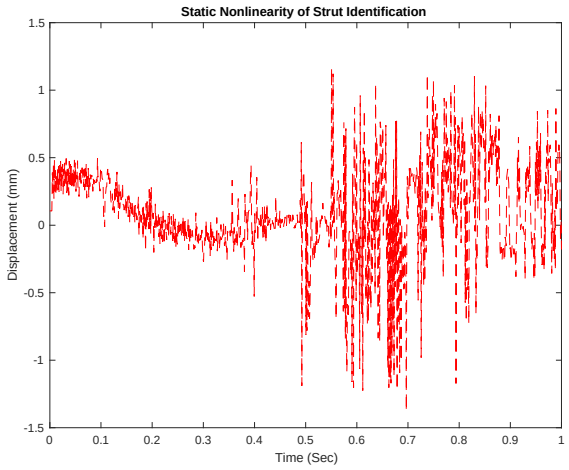

Fig. 12. Static nonlinearity of Weiner model on strut.

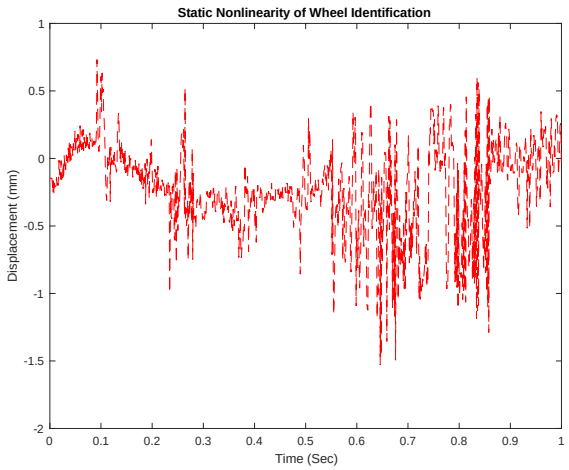

Fig. 13. Static nonlinearity of Weiner model on wheel.

DOI:10.4186/ej.2022.26.1.25

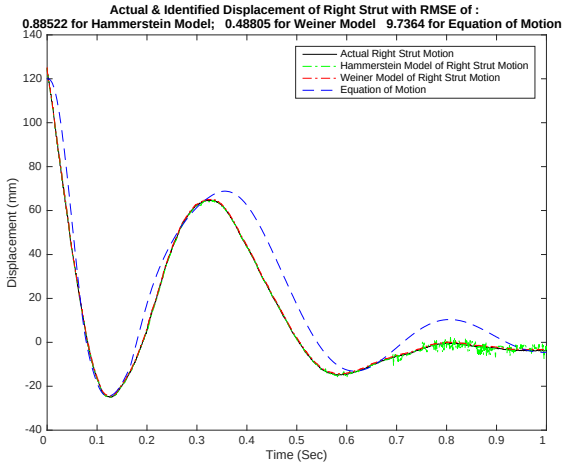

Fig. 14. Motion of the right strut from a 300 mm drop test, showing actual right strut motion, Hammerstein model identification, proposed Weiner model identification, and motion from the governing equation.

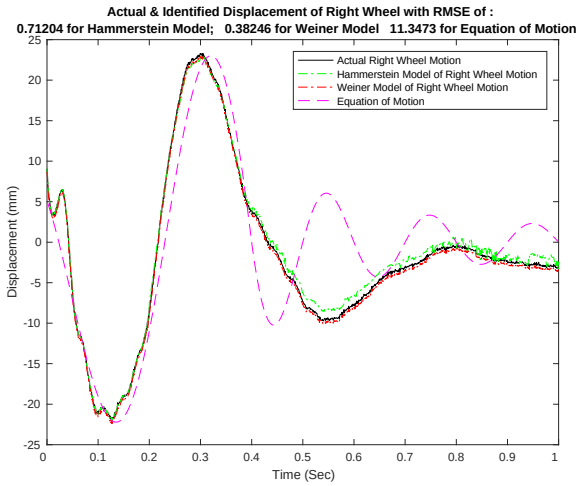

Fig. 15. Motion of the right wheel from a 300 mm drop test, showing actual right strut motion, Hammerstein model identification, proposed Weiner model identification, and motion from the governing equation.

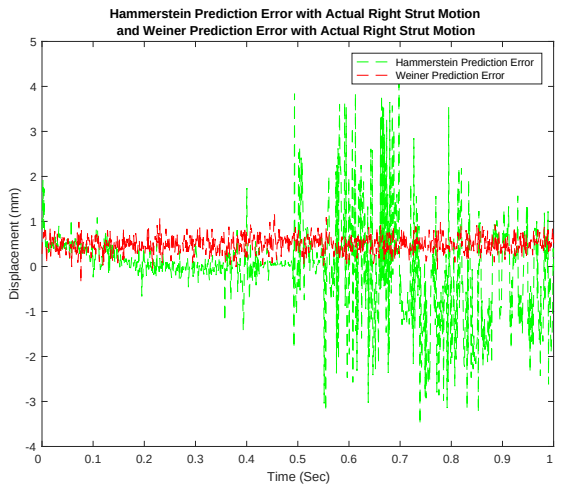

Fig. 16. Relative error of Hammerstein's prediction with the actual right strut motion and relative error of Weiner's prediction with the actual right strut motion.

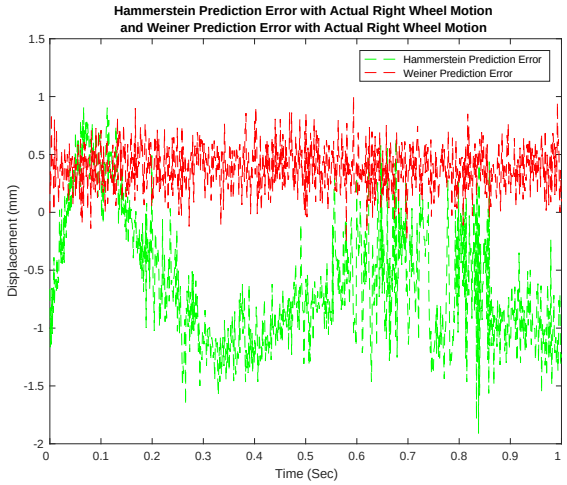

Fig. 17. Relative error of Hammerstein's prediction with the actual right wheel motion and relative error of Weiner's prediction with the actual right wheel motion.

6. Conclusion

This article presents a study of the drop test dynamics of an amphibious airplane using different identification models. With the Gaussian radial basis as a kernel function, the Hammerstein model may be recognized using the LS-SVM identification approach. To identify the model parameters, a constraint convex optimization problem is built up and solved using the KKT condition. However, because the noise in the model input is translated into an infinite dimension, which is a very nonlinear mapping and thus leads to a drastically varied mapping in the hyperplane, this approach cannot be used to identify the Weiner model.

A new approach for estimating the parameters of the Weiner model is proposed to determine the dynamic of the landing gear drop test. The linear parameters of the model could be estimated by utilizing inputs with small magnitudes. Then, using the same LS-SVM approach that was used for Hammerstein model identification, the static nonlinearity function can be determined from the output of the estimated linear portion and the output of the real model. The root mean square error (RMSE) of the suggested Weiner model is relatively low, indicating that the identification model has improved accuracy and dependability.

A full-scale light amphibious aircraft drop test experiment is carried out in line with the ASTM F-2245 standard. At a drop height of 300 mm, the maximum impact loading of 4.8 G is achieved. The main landing gear shock strut absorbs the impact force and balances the aircraft in less than 2 seconds. In terms of estimating strut and wheel displacement output, the proposed Weiner identification model outperforms both the Hammerstein model and the prediction from the governing equation of motion. Nonetheless, the investigation of the Wiener-Hammerstein and Hammerstein-Wiener models for identifying drop dynamics is also intriguing, as is the on-line identification application, both of which could potentially be future research topics to improve system identification performance and to determine whether or

not it is feasible to implement the control algorithm in the system.

Acknowledgments

The author wishes to thank Pongsak HONGNGERN, CEO of Spline Engineering and Construction Co., Ltd., as well as the company's support staff, for their contributions to the development of the test rig that was utilized in this work. The Department of Mechanical and Aerospace Engineering, King Mongkut's University of Technology and National Business (KMUTNB), and Thailand Science Scientific and Innovation (TSRI) are also appreciated for their research cooperation, technical help, and financial support during the project.

References

[1] L. Ljung, *System Identification: Theory for the User*. Upper Saddle River: Prentice Hall, 1999.

[2] J. Schoukens and R. Pintelon, *Identification of Linear Systems: A Practical Guideline to Accurate Modeling*. Elsevier, 2014.

[3] L. A. Mora and J. E. Amaya, "A new identification method based on open loop step response of overdamped system," *RIAI - Revista Iberoamericana de Automatica e Informatica Industrial*, vol. 14, no. 1, pp. 31–43, 2017.

[4] T. Liu, Q.-G. Wang, and H.-P. Huang, "A tutorial review on process identification from step or relay feedback test," *Journal of Process Control*, vol. 23, no. 10, pp. 1597–1623, 2013.

[5] P. V. Overschee and B. de Moor, *Subspace Identification for Linear Systems: Theory Implementation Applications*. Germany: Springer Science & Business Media, 2012.

[6] L. Ljung, *System Identification: Theory for the User, Prentice Hall Information and System Sciences Series*. NJ, USA: Prentice-Hall, 1999.

[7] R. S. Esfandiari and B. Lu, *Modeling and Analysis of Dynamic Systems*. CRC Press, 2014.

[8] D. C. Karnopp, D. L. Margolis, and R. C. Rosenberg, *System Dynamics: Modeling, Simulation, and Control of Mechatronic Systems*, 5th ed. John Wiley & Sons, 2012.

[9] J. Bonilla, L. R. Calle, A. De La and S. Dormido, "Dynamic model of a molten salt-gas heat recovery system for a hybrid renewable solar thermal power plant," *RIAI - Revista Iberoamericana de Automatica e Informatica Industrial*, vol. 14, no. 1, pp. 70–81, 2017.

[10] A. Janczak, *Identification of Nonlinear Systems Using Neural Networks and Polynomial Models: A Block-Oriented Approach*. Springer Science & Business Media, 2004, vol. 310.

[11] F. Giri and E. W. Bai, *Block-Oriented Nonlinear System Identification*. Berlin, Germany: Springer, 2010.

[12] F. J. Doyle, R. K. Pearson, and B. A. Ogunnaike, *Identification and Control Using Volterra Models*. New York, NY: Springer, 2012.

[13] J. J. E. Oviedo, J. P. Vandewalle, and V. Wertz, *Fuzzy Logic, Identification and Predictive Control*. Springer Science & Business Media, 2006.

[14] S. A. Billings, *Nonlinear System Identification: NARMAX Methods in the Time, Frequency, and Spatio-Temporal Domains*. Chichester, UK, John Wiley & Sons, 2013.

[15] J. A. Suykens and J. P. Vandewalle, *Nonlinear Modeling: Advanced Black-Box Techniques*. New York, NY: Springer Science Business Media, 2012.

[16] F. Jurado, "A method for the identification of solid oxide fuel cells using a Hammerstein model," *Journal of Power Sources*, vol. 154, no. 1, pp. 145–152, 2006.

[17] S. Boubaker, "Identification of nonlinear Hammerstein system using mixed integer-real coded particle swarm optimization: Application to the electric daily peak-load forecasting," *Nonlinear Dynamics*, vol. 90, no. 2, pp. 797–814, 2017.

[18] M. S. Gaya, M. U. Zango, and L. A. Yusuf, "Estimation of turbidity in water treatment plant using Hammerstein-Wiener and neural network technique," *Indonesian Journal of Electrical Engineering and Computer Science*, vol. 5, no. 3, pp. 666–672, 2017.

[19] A. Buscarino, C. Corradino, L. Fortuna, M. L. Apicella, G. Mazzitelli, and M. G. Xibilia, "Temperature model identification on FTU liquid lithium limiter," in *Proceedings of the 42nd Conference of the Industrial Electronics Society, IECON 2016*, pp. 6380–6384.

[20] M. R. S. Mohammadi, R. Matos, and C. Rebelo, "Bobtail bolt preload loss in wind turbine tower prototype: Hammerstein-wiener identification model," *CE Papers*, vol. 10, pp. 175–184, 2017.

[21] E.-W. Bai, Z. Cai, S. Dudley-Javoroski, and R. K. Shields, "Application of Wiener-Hammerstein system identification in electrically stimulated paralyzed skeletal muscle modeling," *in Proceedings of the 47th IEEE Conference on Decision and Control*, CDC 2008, Mexico, December 2008, pp. 3305–3310.

[22] E.-W. Bai, Z. Cai, S. Dudley-Javoroski, and R. K. Shields, "Identification of a modified Wiener-Hammerstein system and its application in electrically stimulated paralyzed skeletal muscle modeling," *Automatica*, vol. 45, no. 3, pp. 736–743, 2009.

[23] P. Dewhirst, D. M. Simpson, N. Angarita, R. Allen, and P. L. Newland, "Wiener-Hammerstein parameter estimation using differential evolution," in *International Conference on Bio-inspired Systems and Signal Processing*, January 2010, pp. 271–276.

[24] J. A. Oliver, R. Prieto, J. A. Cobos, O. García, and P. Alou, "Hybrid Wiener-Hammerstein structure for grey-box modeling of dc-dc converters," in *Proceedings of the 24th Annual IEEE Applied Power Electronics Conference and Exposition*, APEC, USA, February 2009, pp. 280–285.

[25] A. Haryanto and K.-S. Hong, "Maximum likelihood identification of Wiener-Hammerstein models," *Mechanical Systems and Signal Processing*, vol. 41, no. 1-2, pp. 54–70, 2013.

[26] I. Benyó, J. Kovács, J. Mononen, and U. Kortela, "Modelling of steam temperature dynamics of a superheater," *International Journal of Simulation: Systems, Science and Technology*, vol. 6, no. 6, pp. 3–9, 2005.

[27] M. J. Korenberg and I. W. Hunter, "The identification of nonlinear biological systems: Lnl cascade models," *Biological Cybernetics*, vol. 55, no. 2-3, pp. 125–134, 1986.

[28] I. C. Gómez, A. Jutan, and E. Baeyens, "Wiener model identification and predictive control of a pH neutralisation process," *IEE Proceedings Control Theory and Applications*, vol. 151, no. 3, pp. 329–338, 2004.

[29] S. Li and Y. Li, "Model predictive control of an intensified continuous reactor using a neural network Wiener model," *Neurocomputing*, vol. 185, pp. 93–104, 2016.

[30] M. Lawryńczuk, "Nonlinear predictive control for Hammerstein–Wiener systems," *ISA transactions*, vol. 55, pp. 49–62, 2015.

[31] Q. Zhang, Q. Wang, and G. Li, "Nonlinear modeling and predictive functional control of Hammerstein system with application to the turntable servo system," *Mechanical Systems and Signal Processing*, vol. 72-73, pp. 383–394, 2016.

[32] M. Lawryńczuk, "Nonlinear predictive control of dynamic systems represented by Wiener–Hammerstein models," *Nonlinear Dynamics*, vol. 86, no. 2, pp. 1193–1214, 2016.

[33] S.A. Billings, and S. Y. Fakhouri, "Identification of systems containing linear dynamic and static nonlinear elements," *Automatica*, vol. 18, no. 1, pp. 15–26., 1982.

[34] F. Giri and E. W. Bai, *Block-Oriented Nonlinear System Identification*. Berlin, Germany: Springer, 2010.

[35] P. Lopes dos Santos, J. A. Ramos, and L. J. Martins de Carvalho, "Identification of a benchmark Wiener-Hammerstein: A bilinear and Hammerstein-bilinear model approach," *Control Engineering Practice*, vol. 20, no. 11, pp. 1156–1164, 2012.

[36] V. Vapnik, *Estimation of Dependences Based on Empirical Data*. Nauka, Moscow, 1979.

[37] Vapnik, V., *The Nature of Statistical Learning Theory*. New York: Springer-Verlag, 1995.

[38] N. Cristianini and J. Shawe-Taylor, *An Introduction to Support Vector Machines and Other Kernel-Based Learning Method*. England, Cambridge University Press, 2000.

[39] S. Totterman and H. Toivonen, "Support vector method for identification of Weiner models," *Journal of Process Control*, vol. 19, pp. 1174-1181, 2009.

[40] I. Goesthals, K. Pelckmans, J. Suykens, and B. Moor, "Identification of MIMO Hammerstein in models using least squares support vector machines," *Automatica*, vol. 4, no. 1, pp. 1263-1272, 2005.

[41] V.-H. Truong and H.-A. Pham, "Support vector machine for regression of ultimate strength of trusses: A comparative study," *Eng. J.*, vol. 25, no. 7, pp. 157-166, Jul. 2021.

[42] A. Dixit, A. Mani, and R. Bansal, "Feature selection for text and image data using differential evolution with svm and naïve Bayes classifiers," *Eng. J.*, vol. 24, no. 5, pp. 161-172, Sep. 2020.

[43] J. Resendiz-Trejo, W. Yu, and X. Li, "Support vector machine for nonlinear system online identification," in *3rd IEEE ICEEE*, 2006, pp. 1-4.

[44] F. Viana, V. Steffen, M. Zanini, S. Magalhaes, and L. Goes, "Identification of a nonlinear landing gear model using nature-inspired optimization," *Shock and Vibrartion*, vol. 15, pp. 257-272, 2008.

[45] M. Tarhouni, K. Laabidi, M. Lahmari-Ksouri, "System identification based on multi-kernel least square support," in *Proceedings of the International Conference on Fuzzy Computation and 2nd International Conference on Neural Computation*, 2010, pp. 310-315.

[46] T. Falck, P. Dreesen, K. Brabanter, K. Pelckmans, B. DeMoor, and J. Suykens, "Least-squares support vector machines for the identification of Weiner Hammerstein systems," *Control Engineering Practice*, vol. 20, pp. 1165–1174, 2012.

[47] J. Sjoberg, L. Lauwers, and J. Schoukens, "Identification of Wiener-Hammerstein models: Two algorithms based on the best slit of a linear model applied to the SYSID'09 benchmark problem," *Control Engineering Practice*, vol. 20, pp. 1119–1125, 2012.

[48] Y. Ding, X. Wei, H. Nie, and Y. Li, "Discharge coefficient calculation method of landing gear shock absorber and its influence on drop dynamics," *Journal of Vibroengineering*, vol. 20, no. 7, pp. 2550-2561, 2018.

[49] S. Ning, F. Yongchun, Z. Yudong, and M. Bojun, "A novel kinematic coupling-based trajectory planning method for overhead cranes", *IEEE/ASME Trans. Mechatronics*, vol.17, pp.166–173, 2012.

[50] B. Milwizky and E. F. Cook, "Analysis of landing gear behavior," TN 2755, Aeronautical Laboratory, Langley Field, VA, USA, 1952.

[51] F. Yu, Z. Maon, M. Jia, and P. Yuan, "Recursive parameter identification of Hammerstein Wiener systems with measurement noise," *Signal Processing*, vol. 105, pp. 137-147, 2014.

[52] S. Jing, "Identification of a deterministic Wiener system based on input least squares algorithm and direct residual method," *International Journal of Modelling, Identification and Control*, vol. 34, no. 3, pp. 208 – 216, 2020.

[53] T. Hastie, R. Tibshirani, and J. Friedman, *The Elements of Statistical Learning*. Heidelberg: Springer, 2001.

[54] S. Chinvorarat and P. Vallikul, "A novel retractable landing gear of a light amphibious airplane design, synthesis, analysis, and implementation," *Aircraft Engineering and Aerospace Technology*, vol. 93, no. 10, pp. 1547-1558, 2021.

DOI:10.4186/ej.2022.26.1.25

Sinchai Chinvorarat received his Ph.D. in Mechanical Engineering in 1999 from Old Dominion University, USA. He is currently an Associate Professor in the Department of Mechanical and Aerospace Engineering at KMUTNB, Thailand. His research interests include Automatic Control Engineering, Aeronautics, System Identification, Power Plant Design and Commissioning. He has published many research articles in the national and international journals.